Journal of Solid State Chemistry **168,** 149–155 (2002)
doi:10.1006/jssc.2002.9703

Crystal Chemistry and Magnetic Properties of $SeCu_{1-x}Zn_xO_3$ ($0 \leq x \leq 1$) Perovskites

R. Escamilla,*,† J. M. Gallardo-Amores,* E. Morán,* and M. A. Alario-Franco*,[1]

*Laboratorio Complutense de Altas Presiones, Departamento de Química Inorgánica, Facultad de Ciencias Químicas, Universidad Complutense, 28040-Madrid, Spain; and †Instituto de Investigaciones en Materiales, Universidad Nacional Autónoma de México, 04510 México D.F., México

Received March 1, 2002; in revised form June 26, 2002; accepted July 16, 2002

The effects of zinc substitution in the structural and magnetic properties of the orthorhombic solid solution $SeCu_{1-x}Zn_xO_3$ have been studied. Rietveld refinements of the X-ray diffraction patterns indicate that the zinc ions occupy the copper sites. This replacement induces some changes in the Cu–O bond lengths and $\langle$ Cu–O–Cu $\rangle$ bond angles. Magnetization vs temperature measurements show a fast decrease in the Weiss constant that reveals a direct quadratic relationship with the increase of the average $\langle$ Cu–O–Cu $\rangle$ bond angle. Besides, the introduction of a non-magnetic cation in the B-positions in the structure of $SeCu_{1-x}Zn_xO_3$ system, progressively decreases the ferromagnetic interactions. © 2002 Elsevier Science (USA)

Key Words: **perovskites; selenites; high pressure; copper oxides; ferromagnetism; Rietveld refinement.**

INTRODUCTION

Transition-metal oxides with the perovskite-type ABO_3 structure have generated a great deal of interest since the early 1950s, due to the chemical versatility and the variety of structural, electrical and magnetic properties that they display (1–3). In the aristotype (Fig. 1a), i.e., the ideal perovskite, the A cation is surrounded by 12 anions at an equal distance. However, only a handful of materials have the ideal cubic symmetry under ambient conditions, such as $SrTiO_3$; most, including the mineral perovskite, $CaTiO_3$, being distorted in different ways (4).

The distortion of perovskite-type ABO_3 structure usually arises from a mismatch in the size of the A and B cations and its common manifestation involves rotation and tilt of the $[BO_6]$ octahedra. This tilting can result in significant anion displacements, even if the cation displacements as well as the distortion of the unit-cell are rather small. A classic example is the orthorhombic perovskite $GdFeO_3$ where it results in $\langle$ Fe–O–Fe $\rangle$ bond angles in the 150–180° range (5, 6). Another example, more relevant to this paper, is the $SeMO_3$ family of phases (M = Mg, Mn, Co, Ni, Cu, and Zn), which can only be synthesized at high pressure (7). In this structure (Fig. 1b), the small Se^{4+} ion, with a strong covalent character, attracts three out of the 12 surrounding oxygens, while the remaining are far apart and linked to other selenium and copper ions. Thus, a $[Se–O_3]^{2-}$ group, rather than a Se^{4+} ion surrounded by 12 oxygens, is the usual component of the structure; moreover, the Se^{4+} species carries a non-bonded or "inert" s-electron pair which also plays an important role because of its peculiar stereochemistry and high polarizability (Fig. 1c). In addition to the above-mentioned tilting, in the $SeCuO_3$, the CuO_6 octahedra also show a large distortion, with different Cu–O bond lengths, due to the Jahn–Teller (JT) effect in Cu^{2+} (d^9). In this structure, Kohn *et al.* recognize that there are two distinct bond angles due to an antiferrodistortive ordering of the JT elongation. These are labeled $\langle$ Cu–O(1)–Cu $\rangle$, along the b-axis and labeled $\langle$ Cu–O(2)–Cu $\rangle$, in the ac plane (7).

Regarding the properties, these authors have shown that the $SeCuO_3$ phase is ferromagnetic with a Weiss constant (θ_w) of 26 K. Both in experimental and theoretical studies, such as the Kramers–Anderson model or the Anderson–Goodenough–Kanemori (AGK) rules for 3d perovskites with unpaired electrons in e_g orbitals, it has been reported that the magnetic interactions change from antiferromagnetic (AFM) to ferromagnetic (FM) as the $\langle$ B–O–B $\rangle$ bond angle varies from 180 to 90° (8, 9). Recently, Subramanian *et al.* (10) have shown that in the $Se_{1-x}Te_xCuO_3$ system, there is an FM (for $x = 0.0$) to AFM ($x = 1.0$) transition that appears to be controlled by a single microscopic parameter, the $\langle$ Cu–O(2)–Cu $\rangle$ bond angle, allowing for the first time a precise determination of the crossover angle (127 ± 0.5°) between FM and AFM superexchange.

To our knowledge, the effects of the replacement of the B cation in this perovskite has not yet been studied and

[1] To whom correspondence should be addressed. Fax: +34-1-394-43-52/43-38. E-mail: maaf@quim.ucm.es, rauleg@servidor.unam.mx.

0022-4596/02 $35.00

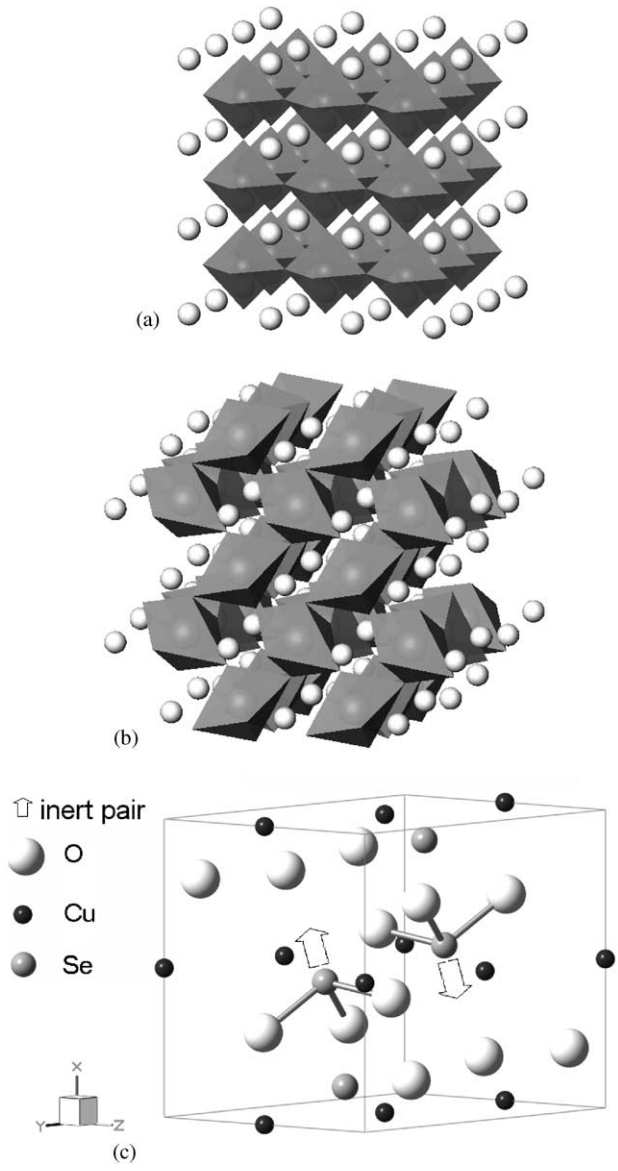

FIG. 1. (a) Projection of the ideal perovskite ABO_3 structure. (b) Projection of the crystal structure of orthorhombic $SeMO_3$ (M = Cu, Zn) showing the octahedral arrangement along *ac* plane. (c) Structural detail showing the presence of selenite $[SeO_3]^{2-}$ groups: each selenium carries a non-bonding electron pair (symbolized by an arrow) which points opposite to the neighbor non-bonding pair.

therefore, in order to see the progressive influence of introducing a non-magnetic cation such as Zn^{2+}, in the Cu^{2+} FM interactions, we have carried out a systematic substitution study in the $Se(Cu_{1-x}Zn_x)O_3$ system with $(0 \leq x \leq 1)$. Interestingly enough, the substitution of Cu^{2+} by Zn^{2+} has been explored in other systems, for example, in high-T_c superconductors such as $YBa_2Cu_3O_7$ and this produces dramatic changes in the physical properties (11). The aim of this work is then to correlate the structural and magnetic changes produced upon modification of the Zn contents in the title perovskites which require high-pressure/high-temperature conditions to be synthesized.

EXPERIMENTAL

Different members of the $Se(Cu_{1-x}Zn_x)O_3$ system $(0 \leq x \leq 1)$ have been synthesized from SeO_2, ZnO, and CuO oxides (99.999% purity) mixed in stoichiometric amounts, sealed in gold capsules and heated, under a pressure of 6 GPa, at temperatures of 900–1000°C using a belt-type press. Phase identification of the samples was done with an X-ray diffractometer Siemens D501 using Cu$K\alpha$ radiation and a Ni filter. Intensities were measured in steps of 0.02° for 13 s in the 2θ range 10–80° at room temperature. Crystallographic parameters were refined using a Rietveld refinement program, Rietica version 1.71 (12), with multi-phase capability. Magnetic susceptibilities were measured between 1.7 and 300 K in a Quantum Design XL-SQUID magnetometer in a 10^3 Oe applied field.

RESULTS AND DISCUSSION

These phases can be only prepared under high-pressure and high-temperature conditions probably because pressure is needed to distort the perovskite structure, by tilting of the $[MO_6]$ octahedra, to stabilize the very small Se^{4+} cation in the A site. The color of the samples changes from green ($x = 0$) to white ($x = 1$) while for intermediate values yellowish green phases are obtained. Figure 2 shows the powder X-ray diffraction patterns obtained for the $Se(Cu_{1-x}Zn_x)O_3$ samples. The obtained materials are crystalline and monophasic, showing the distorted perovskite-type $SeCuO_3$ (IDDE no. 31-0479) and $SeZnO_3$ (IDDE no. 31-1473) common structure. These diffraction patterns were Rietveld–fitted using an orthorhombic $\sim\sqrt{2}a_p \times 2a_p \times \sqrt{2}a_p$ $GdFeO_3$-type cell within space group *Pnma* (no. 62) (a_p is the cubic perovskite cell parameter). In the process of refinement, the substitution of Zn ions in the Cu sites was considered. As an example, one of the fitted patterns ($x = 0.1$) is shown in Fig. 3 and no signs of superstructures have been found, meaning that the substitution takes place in a disordered way. Nevertheless, some of the patterns corresponding to $0.2 \leq x \leq 0.8$ samples show a low intensity, additional peak, around $2\theta = 15°$ corresponding to the (110) reflection of SeO_2 (IDDE no. 22-1314) which often appears as a minor impurity and excluded in the Rietveld analysis. The $x = 0.6$ sample also shows a tiny peak around 18° which would correspond to an unidentified phase. Detailed results of the structural refinements are listed in Table 1. Figure 4 shows the changes, at room temperature, of the lattice parameters and the unit-cell volume for the $Se(Cu_{1-x}Zn_x)O_3$ samples as a function of Zn concentration (x). The lattice parameters obtained in this work agree satisfactorily with

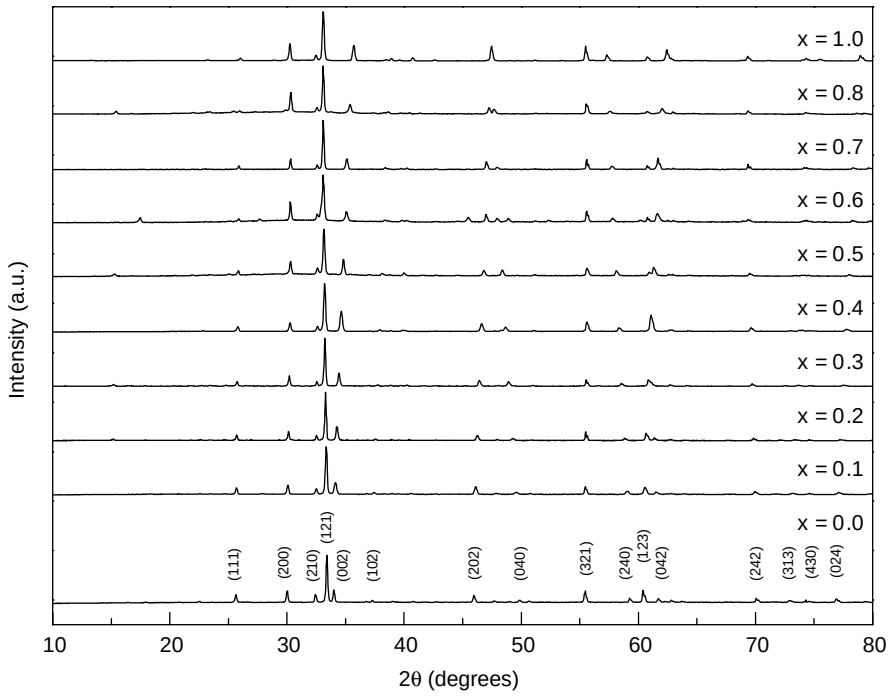

FIG. 2. X-ray diffraction patterns of the $Se(Cu_{1-x}Zn_x)O_3$ ($0 \leq x \leq 1.0$) samples.

the data available in the literature for the end members (7). It can be observed that the *a*-parameter do not change significantly while the *b*-parameter continuously increases (at maximum substitution, that is for the all-zinc end member, the increase is of 5%). On the other hand, the *c*-parameter slightly diminishes as *x* increases. Moreover, for all the compounds presented here, the orthorhombic distortions defined as $b/(a\sqrt{2})$ and $b/(c\sqrt{2})$ ratios vary, in a regular fashion, within the 0.8678–1.0760 range, which corresponds to $SeCuO_3$ and $SeZnO_3$, respectively (see Table 1). Hence, substitution of Cu^{2+} ions by Zn^{2+} ions in a non-ordered way results in an increase of the orthorhombic distortion although it does not cause significant changes in the unit-cell volume ($\sim < 1\%$) (see Table 1) because of a compensation effect. This Vegard's law-like behavior indicates that a complete solid solution exists and the structural and physical properties of the system are expected to change smoothly, may be linearly, on substitution. It is noteworthy that the solid solution limits are broader than in other cuprates with perovskite-related structures, i.e. only 30% Zn^{2+} may replace Cu^{2+} in $YBa_2Cu_3O_7$ (11).

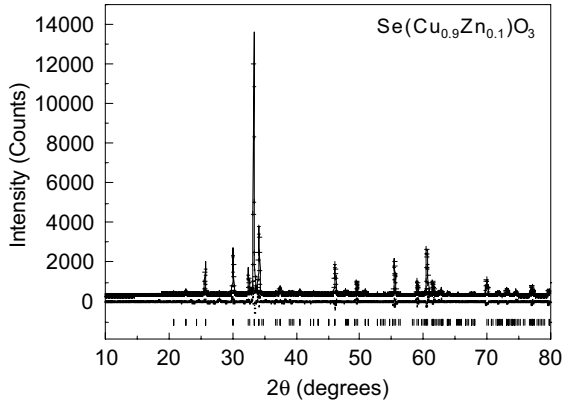

FIG. 3. Rietveld refinement on the X-ray diffraction pattern for the $x = 0.1$ sample. Experimental diagram (dots), calculated pattern (continuous line), their difference (middle line) and calculated peak positions (bottom).

Table 2 compares the *M*–O ($M = Cu/Zn$) bond lengths and $\langle M\text{–O–}M \rangle$ bond angles obtained from the refined atomic positions together with the $[MO_6]$ octahedron distortion for each sample (see Fig. 5). The octahedron distortion is defined as $D_{oct} = 10\,[\Sigma(M-O_i) - (M-O)_{average}]/(M-O)_{average}$ as in Ref. (24). We can observe small, but significant, changes in the *M*–O bond lengths and $\langle M\text{–O–}M \rangle$ bond angles within the $[MO_6]$ octahedra as *x* increases, in spite of the fact that the ionic radii of Cu^{2+} (0.73 Å) and Zn^{2+} (0.72 Å) are quite close (13). In this connection and, as expected by the aforementioned Vegard's law behavior, linear variations are observed. Regarding the distortion of the $[MO_6]$ octahedra, Kohn *et al.* (7) have shown it to be quite large in the $SeCuO_3$ system due to the preference of a JT Cu^{2+} ion for non-octahedral bonding. Distortions of the same type have also been observed in, for example, $KCuF_3$ (14) and $CuTe_2O_5$ (15). Our data for the $SeCu_{1-x}Zn_xO_3$ system,

TABLE 1
Structural Parameters for $SeMO_3$ at 295 K. $M = (Cu_{1-x}Zn_x)$

	$x =$	0.0	0.1	0.2	0.3	0.4	0.5	0.6	0.7	0.8	1.0
	a (Å)	5.9656(3)	5.9502(1)	5.9416(2)	5.9249(9)	5.9166(8)	5.9099(7)	5.8997(2)	5.9047(3)	5.9053(6)	5.9207(5)
	b (Å)	7.3213(4)	7.3632(4)	7.4081(3)	7.4515(1)	7.4949(9)	7.5375(6)	7.5896(3)	7.5971(3)	7.6336(6)	7.6655(4)
	c (Å)	5.2804(2)	5.2601(3)	5.2437(2)	5.2140(9)	5.1895(7)	5.1618(4)	5.1182(4)	5.1176(4)	5.0824(8)	5.0377(5)
	$b/(a\sqrt{2})$	0.8678	0.8750	0.8817	0.8893	0.8957	0.9019	0.9096	0.9098	0.9141	0.9155
	$b/(c\sqrt{2})$	0.9804	0.9898	0.9990	1.0106	1.02124	1.0326	1.0485	1.0497	1.06216	1.0760
	V (Å^3)	230.63(3)	230.46(3)	230.80(3)	230.20(8)	230.13(6)	229.94(6)	229.17(3)	229.57(2)	229.11(5)	228.64(5)
	B_{ovel} (Å^2)	0.64(4)	1.04(15)	1.97(4)	1.47(3)	1.77(5)	0.96(5)	0.78(4)	0.34(3)	1.8(2)	0.03(4)
Se	x	0.0401(6)	0.0387(3)	0.0373(4)	0.0359(3)	0.0345(3)	0.0333(3)	0.0316(3)	0.0304(3)	0.0292(2)	0.0266(3)
	z	0.0030(4)	−0.0002(2)	−0.0034(2)	−0.0066(3)	−0.0098(5)	−0.0132(3)	−0.0081(4)	−0.0115(4)	−0.0149(3)	−0.0161(4)
O(1)	x	0.0791	0.0791	0.0791	0.0791	0.0791	0.0791	0.0792(3)	0.0792(4)	0.0792(3)	0.0793(5)
	z	0.3310(3)	0.3297(4)	0.3284(4)	0.3271(3)	0.3258(3)	0.3249(3)	0.3227(4)	0.3218(3)	0.3209(4)	0.3184(6)
O(2)	x	0.2020(2),	0.2005(1),	0.1986(2),	0.1968(3),	0.1949(4),	0.1931(2),	0.1910(5)	0.1892(5)	0.1874(4)	0.1838(4)
	y	0.0732(2),	0.0738(2),	0.0742(3),	0.0747(3),	0.0753(4),	0.0757(4),	0.0767(3)	0.0771(3)	0.0775(5)	0.0785(3)
	z	0.9060(1)	0.9025(3)	0.8984(4)	0.8943(4)	0.8902(6)	0.8861(4)	0.8823(5)	0.8782(3)	0.8741(3)	0.8661(4)
	R_p (%)	8.8	9.0	11.4	10.7	10.9	7.1	14.4	13.3	15.9	11.8
	R_{wp} (%)	8.5	7.2	8.9	11.3	10.8	5.6	15.4	13.0	14.7	14.1
	χ^2	1.7	2.7	4.1	2.7	1.74	4.4	4.3	2.3	4.8	3.1

Note. Space group: *Pnma* (no. 62). Atomic positions: M (Cu, Zn): $4b(0, 0, \frac{1}{2})$; Se: $4c(x, \frac{1}{4}, z)$; O(1): $4c(x, \frac{1}{4}, z)$; O(2): $8d$ (x, y, z).

shown in Table 2, evidence that the octahedron distortion decreases with increasing (x) (see Fig. 5). This can be associated with the fact that such a substitution does reduce the JT effect characteristic of Cu^{2+}, because the number of JT Cu^{2+} ions decreases; obviously, for $SeZnO_3$ the JT effect is zero, a consequence of the Zn^{2+} ions being, electronically, a closed shell.

On the other hand, Table 3 compares the Se–O crystallographic distances, three minimum lengths between selenium and oxygen ions: $Se–O(1)_i$ and $Se–O(2)_{ii}$ ($\times 2$) being found at approximately 1.71 Å, which indicates strong bonding. Thus, a $[SeO_3]^{2-}$ group rather than a Se^{4+} ion surrounded by 12 oxygens is a basic feature of this structure. Figure 5b plots the average Se–O bond length in this $[SeO_3]^{2-}$ group vs zinc concentration (x) and it does not change for the solid solution studied. This suggests that the substitution of Cu^{2+} ions for Zn^{2+} ions does not affect the $[SeO_3]^{2-}$ group of the $SeCu_{1-x}Zn_xO_3$ structure and so one can consider two different types of bonding: essentially covalent within the selenite anions and more ionic between these and the transition metal ions.

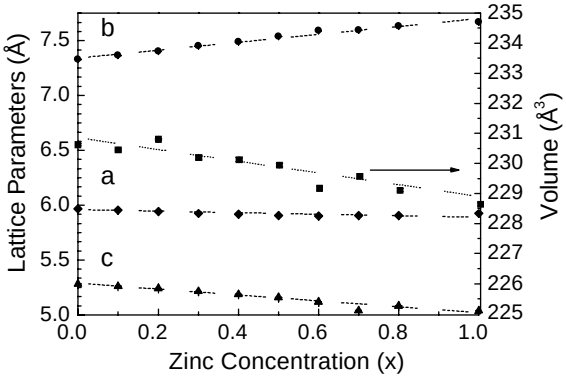

FIG. 4. Crystal lattice parameters and unit cell volumes as a function of zinc concentration (x).

As usual, the geometry of the selenite group in this structure is a trigonal-pyramidal one, as resulting from a tetrahedral configuration around a central atom (Se) with three bonding electron pairs (Se–O) and a non-bonding electron pair occupying the remaining apical position, opposite to the pyramid basal plane. It is also worth mentioning that the three oxygens belonging to the $[SeO_3]^{2-}$ group alternate, up and down, along the Se–Se line; similarly, but oppositely, do the inert pairs (Fig. 1c). Thus, the inert pairs fill the big dodecahedral A position and are assimilated to an oxide ion.

Interestingly enough, if we follow the Galy *et al.* model (17), based on an early idea by Durrant and Durrant (18), which accounts for the stereochemical influence of the non-bonding pairs borne by the so-called $s-p$ elements in a two-below its maximum oxidation state, e.g., Tl^+, Pb^{2+}, Se^{4+}, Bi^{3+}, etc., we can estimate the "degree of non-bonding character"[2] (1 at its maximum) as the ratio of the average distance from the cation to the non-bonding pair (1.22 Å, from Table XI in Ref. 17) to the observed cation–oxygen distance, which in our case is 1.71 Å.This ratio turns out to be 0.71, which fits almost perfectly to the

[2] In French in the original article: "taux en paire non engagé".

TABLE 2
***M*–O Bond lengths (Å), Octahedron Distortion and Angles (deg) between the [*M*–O_6] (*M* = Cu, Zn) for $SeMO_3$**

$x =$	0.0	0.1	0.2	0.3	0.4	0.5	0.6	0.7	0.8	1.0
M–O(1): 2	2.090(1)	2.101(2)	2.112(2)	2.122(4)	2.140(1)	2.142(1)	2.155(2)	2.158(2)	2.177(3)	2.175(3)
M–O(2): 2	2.516(4)	2.490(5)	2.462(5)	2.428(12)	2.389(4)	2.366(3)	2.332(3)	2.310(4)	2.278(4)	2.225(4)
M–O(2): 2	1.921(4)	1.932(5)	1.948(5)	1.960(12)	1.974(4)	1.990(3)	2.006(4)	2.025(3)	2.041(4)	2.080(4)
$\langle M\text{–O}\rangle_{\text{average}}$	2.175	2.174	2.174	2.170	2.167	2.166	2.164	2.164	2.165	2.160
D_{oct}	3.13	2.90	2.65	2.38	2.04	1.85	1.55	1.34	1.12	0.74
M–O(2)–*M*: 4	127.1(1)	127.3(2)	127.6(2)	127.8(8)	127.9(5)	128.3(1)	128.2(3)	128.5(3)	128.7(2)	129.2(3)
M–O(1)–*M*: 2	122.3(1)	122.4(2)	122.5(2)	122.8(8)	123.5(5)	123.3(1)	123.4(2)	123.3(4)	123.6(3)	123.5(4)
$\langle M\text{–O–}M\rangle_{\text{average}}$	125.5	125.7	125.9	126.1	126.4	126.6	126.6	126.8	127.0	127.3

Note. The octahedron distortion is defined as $D_{\text{oct}} = 10\,(\Sigma|(M\text{–O}_i) - \langle M\text{–O}\rangle_{\text{average}}|)/\langle M\text{–O}\rangle_{\text{average}}$ [Ref. 16].

expected "degree of non-bonding character" for Se^{4+}, which is 0.70 (from Table XII in Ref. 17). As remarked by Galy *et al.* only Br^{5+} and Xe^{6+} have a higher inert pair effect degree than Se^{4+}, see Chapter X in Ref. 19.

On the other hand, octahedra are not only distorted but also adopt a tilted position (Fig. 1b). It is well known that tilting of the octahedra is commonly observed in perovskites such as the orthorhombic $GdFeO_3$ (5). Also in the $A_xR_{1-x}MnO_3$ (*R* = rare earth; *A* = Ba, Sr, Ca) system (20, 21), the presence of the tilting is manifested in terms of increases of the ⟨Mn–O–Mn⟩ bond angles due to an *A*-site atom size effect, while, in the $Sr_x(Na_{0.5}Ln_{0.5})_{1-x}RuO_3$ system, the ⟨Ru–O–Ru⟩ bond angle slightly increases as a direct consequence of the charge disorder on the *A*-site (22). Our results of the Rietveld–fit for the $SeCu_{1-x}Zn_xO_3$ system show that the increase in the orthorhombic distortion may be associated to significant changes in the ⟨Cu–O–Cu⟩ bond angles, which are smaller than those in any of the ABO_3 perovskites: the average bond angle (α) changes from 125.5° ($x = 0.0$) to 127.3° ($x = 1.0$) (see Table 2) and this structural feature correlates with the observed magnetic properties.

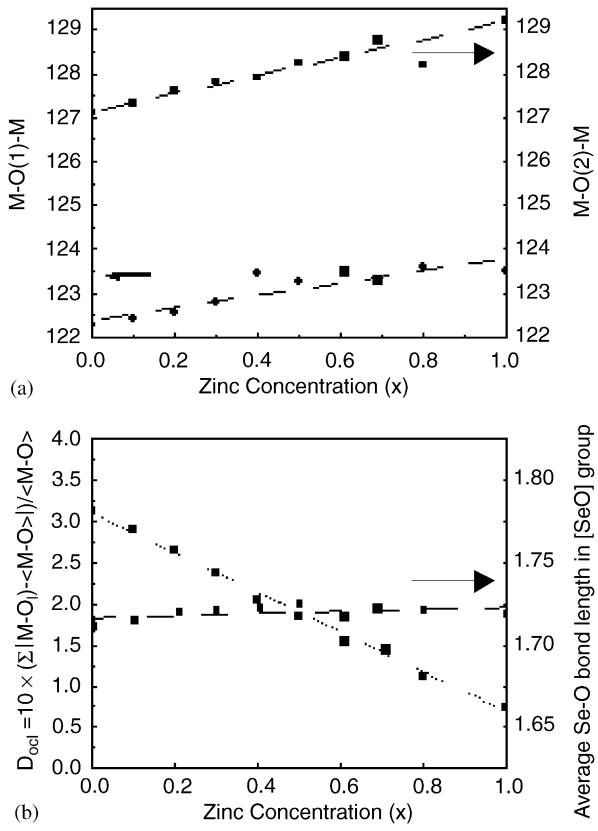

FIG. 5. (a) ⟨*M*–O(1)–*M*⟩ and ⟨*M*–O(2)–*M*⟩ bond angles vs zinc concentration (b) MO_6 octahedron distortion and average Se–O bond length in the $[Se\text{–}O]^{2-}$ group vs zinc concentration (*x*).

Figure 6 shows the magnetization as a function of temperature for the $Se(Cu_{1-x}Zn_x)O_3$ samples: at low temperatures, the $x < 0.8$ materials are ferromagnetic and the observed magnetization and transition temperatures (T_c, determined from the corresponding peaks in the dM/dT curves) decrease upon increasing *x*. Although the magnetization values seem to be different, if they were expressed per mole of copper, the plots would practically overlap for $x < 0.5$. The magnetic moment obtained at saturation is 0.8 μ_B per Cu^{2+}, instead of the expected value of 1 μ_B, as it is usually reported in the literature for this cation. Therefore, the main effect in the magnetic properties produced by the non-magnetic Zn^{2+} replacing of Cu^{2+} is the dilution of the ferromagnetic interactions. Worthy to note, when the system becomes quite diluted ($x > 0.5$), there is a change in the shape of the magnetization curves and no magnetic saturation is achieved. For all materials, the behavior at high temperature (above T_c) is well described by the Curie–Weiss law: $\chi = C/(T - \theta_w)$ where *C* is the Curie constant and θ_w the Weiss constant. The inset of Fig. 6 shows χ^{-1} vs *T* for several samples and it is clear that, while the slope changes for different *x*, θ_w, as determined from a fit to the high-temperature behavior ($T > 100$ K), continuously decreases as the non-magnetic cation is introduced in the structure.

Concerning the correlation between *M*–O–*M* angles and FM–AFM interactions, it was stated that, in the $Se_{1-x}Te_xCuO_3$ system, there exists an FM (for $x = 0.0$) to AFM ($x = 1.0$) transformation that appears to be controlled by a single microscopic parameter, the α_c critical angle

TABLE 3
Se–O Distances (Å), for SeMO_3

$x =$	0.0	0.1	0.2	0.3	0.4	0.5	0.6	0.7	0.8	1.0
Se–O(1)$_{i}$	1.746(3)	1.751(4)	1.757(5)	1.758(6)	1.752(2)	1.766(1)	1.716(2)	1.718(3)	1.732(1)	1.714(5)
Se–O(1)$_{ii}$	2.884(2)	2.878(1)	2.872(4)	2.863(3)	2.854(1)	2.854(4)	2.832(3)	2.834(3)	2.834(4)	2.830(5)
Se–O(1)$_{iii}$	3.330(3)	3.338(2)	3.347(4)	3.351(3)	3.355(3)	3.368(3)	3.367(2)	3.381(2)	3.394(3)	3.421(4)
Se–O(1)$_{iv}$	3.554(4)	3.533(3)	3.512(6)	3.483(5)	3.439(2)	3.427(3)	3.437(3)	3.400(4)	3.388(6)	3.368(3)
Se–O(2)$_{ii}$ ($\times 2$)	1.693(6)	1.694(3)	1.697(3)	1.697(7)	1.702(6)	1.699(4)	1.711(2)	1.713(1)	1.710(3)	1.717(1)
Se–O(2)$_{vi}$ ($\times 2$)	2.812(4)	2.823(6)	2.834(5)	2.845(6)	2.869(1)	2.871(5)	2.879(4)	2.894(4)	2.899(1)	2.909(5)
Se–O(2)$_{iii}$ ($\times 2$)	3.224(5)	3.195(4)	3.168(1)	3.135(2)	3.101(2)	3.077(4)	3.072(3)	3.045(3)	3.023(4)	2.993(4)
Se–O(2)$_{vii}$ ($\times 2$)	3.533(2)	3.546(3)	3.559(4)	3.568(1)	3.582(3)	3.590(2)	3.580(4)	3.592(2)	3.599(9)	3.604(3)
Average Se–O bond length in SeO_3 group[a]	1.711	1.713	1.717	1.717	1.719	1.721	1.713	1.715	1.717	1.716

[a] With Se–O(1)$_{i}$ and Se–O(2)$_{ii}$ ($\times 2$).

($127 \pm 0.5^{\circ}$) (10). Also, in the $R_{1-x}A_xMnO_3$ system (16, 20, 23) the variation in magnetic properties may be basically understood in terms of the change of bond angles. For example, it is observed that decreasing θ_w correlates with changes in the $\langle$ Mn–O–Mn $\rangle$ bond angle. While, in the $Sr_xCa_{1-x}RuO_3$ system (24) it is observed that the value of θ_w decreases in terms of A-site atom size disorder. However, in our Se$(Cu_{1-x}Zn_x)O_3$ system, because solid solution is an "average" situation, instead of considering the two $\langle M$–O–$M \rangle$ angles separately, it is better to use the "average" angle (α) and, in order to find a more in-depth correlation between the crystallographic and magnetic properties of the Se$(Cu_{1-x}Zn_x)O_3$ system, the evolution of θ_w as a function of the average $\langle M$–O–$M \rangle$ bond angle (α) is displayed in the inset of Fig. 7. We observe that:

(a) The Weiss constant, θ_w, decreases with increasing x and it can be extrapolated to zero for $x = 0.8$.

(b) In spite of the fact that the average bond angles are, for the $SeCu_{1-x}Zn_xO_3$ solid solution, smaller than the aforementioned critical angle ($127 \pm 0.5^{\circ}$), the materials remain ferromagnetic down to the low concentration of $\sim 20\%$ of Cu.

The main result of the Zn substitution is then a dilution effect of the ferromagnetic interactions; Zn introduces disorder in the Cu lattice and the compounds become magnetically inhomogeneous. As the average bond angle is increased, the octahedron distortion decreases, a feature which can be ascribed to the introduction of the non-Jahn–Teller Zn^{2+} cation in the structure and in this sense, we observe that the maximum θ_w is achieved for the perovskite-type $SeCuO_3$. On the other hand, we have found a quadratic correlation between the Weiss constant and the average bond angle. The plot is a fit to a law $\theta_w(\alpha) = A + B\alpha + C\alpha^2$ with $A = -11.1 \times 10^4$ K, $B = 0.18 \times 10^4$ K and $C = -0.0007 \times 10^4$ K but the theoretical

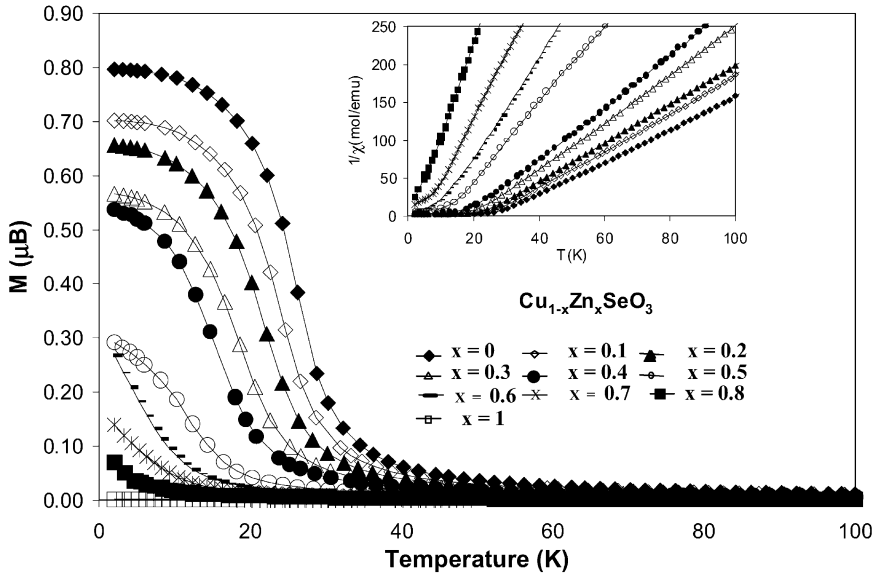

FIG. 6. Magnetization as a function of temperature for the Se$(Cu_{1-x}Zn_x)O_3$ samples. The inset shows the inverse susceptibility χ^{-1} vs T plot.

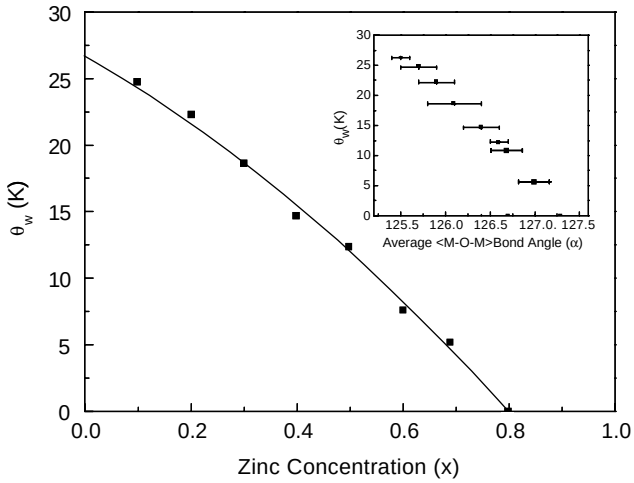

FIG. 7. Weiss constant (θ_w) vs zinc concentration (x). The inset shows the Weiss constant (θ_w) vs average $\langle M\text{–O–}M \rangle$ bond angle plot.

grounds of such an experimental relationship are not yet understood. A more detailed study of the magnetic properties is in progress in order to know if, for instance, the magnetic disorder produces the presence of a spin-glass state for the intermediate compounds.

ACKNOWLEDGMENTS

We would like to thank Dr. Julio Romero for assistance with the magnetic measurements and Prof. R. Sáez-Puche for helpful discussions concerning magnetic results; both of them at the Universidad Complutense de Madrid. This work was supported by DGAPA-UNAM (México), CONACYT (México) and CICYT MAT-98-0729 (Spain).

REFERENCES

1. F. S. Galasso, "Perovskites and High T_c Superconductors." Gordon & Breach, New York, 1990.
2. J. B. Goodenough, *Phys. Rev.* **100,** 564 (1955).
3. N. Tsuda, K. Nasu, A. Yanase, and K. Siratori, "Electronic Conduction in Oxides." Springer, Berlin, 1991.
4. B. J. Kennedy, C. J. Howard, and B. C. Chakoumakos, *J. Phys. Condens. Matter* **11,** 1479 (1999).
5. S. Geller, *J. Chem. Phys.* **24,** 1236 (1956).
6. S. Geller and E. A. Wood, *Acta Crystallogr.* **9,** 563 (1956).
7. K. Kohn, K. Inoue, O. Horie, and S. Akimoto, *J. Solid State Chem.* **18,** 27 (1976).
8. P. W. Anderson, *Phys. Rev.* **79,** 705 (1950).
9. J. Kanemori, *J. Phys. Chem. Solids* **10,** 87 (1959).
10. M. A. Subramanian, A. P. Ramirez, and W. J. Marshall, *Phys. Rev. Lett.* **82,** 1558 (1999).
11. T. J. Kistenmacher, *Phys. Rev. B* **38,** 8862 (1988).
12. C. J. Howard, B. A. Hunter, and D. A. J. Swinkels, *Rietica. IUCR Powder Diffraction* **22,** 21 (1997).
13. R. D. Shannon. *Acta Crystallogr. A* **32,** 751 (1976).
14. A. Okazaki and Y. Suemune, *J. Phys. Soc. Jpn.* **16,** 176 (1961).
15. K. Hanke, V. Kupcik, and O. Lindqvist, *Acta Crystallogr. B* **29,** 963 (1973).
16. C. Zener, *Phys. Rev.* **82,** 403 (1951).
17. J. Galy, G. Meunier, S. Anderson, A. Åström, *J. Solid State Chem.* **13,** 142 (1975).
18. P. J. Durrant, and B. Durrant, "General and Inorganic Chemistry," p. 647. Longmans & Green and Co. Ltd, London, 1962.
19. B. G. Hyde and S. Anderson, "Inorganic Crystal Structures." Wiley Interscience. John Wiley & Sons, New York, 1989.
20. J. L. García-Muñoz, J. Fontcuberta, M. Suaaidi, and X. Obradors, *J. Phys. Condens. Matter* **8,** L787 (1996).
21. J. Blasco, C. Ritter, J. García, J. M. de Teresa, J. Pérez-Cacho, and M. R. Ibarra, *Phys. Rev. B* **62,** 9 (2000).
22. T. He, Q. Huang, and R. J. Cava, *Phys. Rev. B.* **63,** 24,402 (2001).
23. L. M. Rodríguez-Martínez and J. P. Attfield, *Phys. Rev. B* **63,** 24,424 (2000).
24. Mazin and D. J. Singh, *Phys. Rev. B* **56,** 2556 (1997).